Journal: Monthly Notices of the Royal Astronomical Society
Article doi: 10.1093/mnras/stw1738
Article title: New orbits of irregular satellites designed for the predictions of stellar occultations up to 2020, based on thousands of new observations
First Author: A. R. Gomes-Júnior
Corr. Author: M. Assafin

INSTRUCTIONS

We encourage you to use Adobe's editing tools (please see the next page for instructions). If this is not possible, please list clearly in an e-mail. Please do not send corrections as track changed Word documents.

Changes should be corrections of typographical errors only. Changes that contradict journal style will not be made.

These proofs are for checking purposes only. They should not be considered as final publication format. The proof must not be used for any other purpose. In particular we request that you: do not post them on your personal/institutional web site, and do not print and distribute multiple copies. Neither excerpts nor all of the article should be included in other publications written or edited by yourself until the final version has been published and the full citation details are available. You will be sent these when the article is published.

1. **Licence to Publish:** Oxford Journals requires your agreement before publishing your article. If you haven't already completed this, please sign in with your My Account information and complete the online licence form. Details on how to do this can be found in the Welcome to Oxford Journals email.
2. **Permissions: Permission to reproduce any third party material in your paper should have been obtained prior to acceptance. If your paper contains figures or text that require permission to reproduce, please inform me immediately by email.**
3. **Author groups:** Please check that all names have been spelled correctly and appear in the correct order. Please also check that all initials are present. Please check that the author surnames (family name) have been correctly identified by a pink background. If this is incorrect, please identify the full surname of the relevant authors. Occasionally, the distinction between surnames and forenames can be ambiguous, and this is to ensure that the authors' full surnames and forenames are tagged correctly, for accurate indexing online.
4. **Figures:** If applicable, figures have been placed as close as possible to their first citation. Please check that they are complete and that the correct figure legend is present. Figures in the proof are low resolution versions that will be replaced with high resolution versions when the journal is printed.
5. **Missing elements:** Please check that the text is complete and that all figures, tables and their legends are included.
6. **Special characters and equations:** Please check that special characters, equations and units have been reproduced accurately.
7. **URLs:** Please check that all web addresses cited in the text, footnotes and reference list are up-to-date.
8. **Funding:** If applicable, any funding used while completing this work should be highlighted in the Acknowledgements section. Please ensure that you use the full official name of the funding body.

AUTHOR QUERIES - TO BE ANSWERED BY THE CORRESPONDING AUTHOR

The following queries have arisen during the typesetting of your manuscript. Please answer these queries by marking the required corrections at the appropriate point in the text.

Query No.	Nature of Query	Author's Response
Q1	Author: The figures have been processed according to the information you entered during the submission of your manuscript. Please note that there is a charge of £200 (+VAT) for publishing in colour in print. There is no charge to publish figures in black and white in print and in colour online. If you have already requested print colour figures or have now decided to have print colour figures please confirm that you are willing to pay the £200 (+VAT) charge. You will be invoiced upon publication. If you do not wish to have your figures published in colour in print, please confirm. Black and white versions of figures are provided at the end of the paper. Please check the black and white versions to assess their quality for the print version of the of the journal, please contact us if you have any concerns.	
Q2	Author: Please supply email addresses for between one and three authors who are willing to correspond with readers and for their email address to be included in the article	
Q3	Author: To check that we have your surnames correctly identified and tagged (e.g. for indexing), we have coloured pink the names that we have assumed are surnames. If any of these are wrong, please let us know so that we can amend the tagging.	
Q4	Author: Please note that citations are not permitted to appear in the Abstract with the year included; nor are citations that are within brackets allowed in the Abstract. Changes OK?	
Q5	Author: Please note that citations are not permitted to appear in the Abstract with the year included; nor are citations that are within brackets allowed in the Abstract. Changes OK?	
Q6	Author: If you refer to any data bases in your paper, please note the journal policy for properly crediting those responsible for compiling the data base. Rather than citing only a URL, if at all possible please also cite a reference (and include it in the reference list), or if a reference is not available then the names of those who compiled the data base. Note that some data bases do provide guidelines on how they should be cited – please check for these and follow them in your paper where appropriate.	
Q7	Author: The MNRAS list of approved key words has been revised and updated. The new list is appended to these proofs. If you had previously selected key words from the old list, please now check them carefully against the new list in case they need to be changed, or there are new ones that you would like to add. If you had not previously selected key words from the MNRAS approved list, please now choose up to six from the new list.	
Q8	Author: Journal style rules state that vectors and tensors must be written in bold italic ($\boldsymbol{X}$), matrices must be written in bold san serif ($\boldsymbol{\mathsf{X}}$) and scalars must be written in italic (X). Please check carefully that the notations used throughout this paper are correct.	

Query No.	Nature of Query	Author's Response
Q9	Author: As per journal style, the running head short title of a paper must not exceed 45 characters (including spaces between words and punctuation marks); please supply an alternative short title of up to 45 characters (including any spaces between words and punctuation marks) that can be used instead.	
Q10	Author: Please check the figures in the PDF proof carefully.	
Q11	Author: Please provide the name of publisher and its location if possible.	
Q12	Author: Please update the reference if possible.	

MAKING CORRECTIONS TO YOUR PROOF

These instructions show you how to mark changes or add notes to the document using the Adobe Acrobat Professional version 7 (or onwards) or Adobe Reader X (or onwards). To check what version you are using go to **Help** then **About**.
The latest version of Adobe Reader is available for free from get.adobe.com/reader.

Displaying the toolbars

Adobe Professional X, XI and Reader X, XI

Select **Comment, Annotations and Drawing Markups.**
If this option is not available, please let me know so that I can enable it for you.

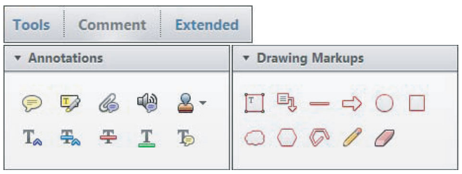

Acrobat Professional 7, 8 and 9

Select **Tools, Commenting, Show Commenting Toolbar**.

Using Text Edits

This is the quickest, simplest and easiest method both to make corrections, and for your corrections to be transferred and checked.

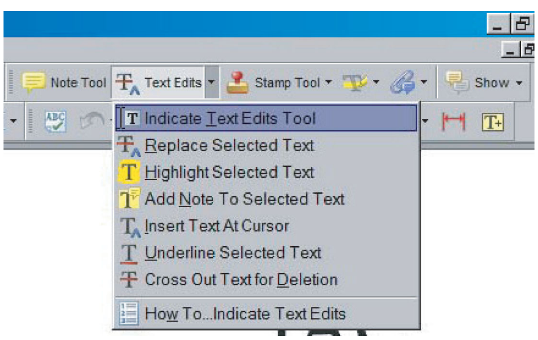

1. Click **Text Edits**
2. Select the text to be annotated or place your cursor at the insertion point.
3. Click the **Text Edits** drop down arrow and select the required action.

You can also right click on selected text for a range of commenting options.

Pop up Notes

With *Text Edits* and other markup, it is possible to add notes. In some cases (e.g. inserting or replacing text), a pop-up note is displayed automatically.

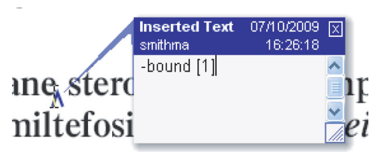

To **display** the pop-up note for other markup, right click on the annotation on the document and selecting **Open Pop-Up Note**.

To **move** a note, click and drag on the title area.

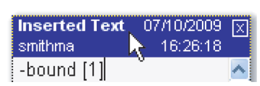

To **resize** of the note, click and drag on the bottom right corner.

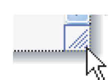

To **close** the note, click on the cross in the top right hand corner.

To **delete** an edit, right click on it and select **Delete**. The edit and associated note will be removed.

SAVING COMMENTS

In order to save your comments and notes, you need to save the file (**File, Save**) when you close the document.
A full list of the comments and edits you have made can be viewed by clicking on the Comments tab in the bottom-left-hand corner of the PDF.

MNRAS (2016)
Advance Access publication 2016 July 19

doi:10.1093/mnras/stw1738

New orbits of irregular satellites designed for the predictions of stellar occultations up to 2020, based on thousands of new observations

A. R. Gomes-Júnior,[1★] M. Assafin,[1†] L. Beauvalet,[2,3] J. Desmars,[4] R. Vieira-Martins,[1,2,5†] J. I. B. Camargo,[2,5] B. E. Morgado[1,2] and F. Braga-Ribas[2,6]

[1]Observatório do Valongo/UFRJ, Ladeira Pedro Antônio 43, CEP 20080-090 Rio de Janeiro, RJ, Brazil
[2]Observatório Nacional/MCTI, R. General José Cristino 77, CEP 20921-400 Rio de Janeiro, RJ, Brazil
[3]Observatoire de Paris/SYRTE, 77 Avenue Denfert Rochereau, 75014 Paris, France
[4]IMCCE, Observatoire de Paris, PSL Research University, CNRS, Sorbonne Universités, UPMC Univ Paris 06, Univ. Lille, 77 Avenue Denfert Rochereau, 75014 Paris, France
[5]Laboratório Interinstitucional de e-Astronomia – LIneA, Rua Gal. José Cristino 77, 20921-400 Rio de Janeiro, RJ, Brazil
[6]Federal University of Technology – Paraná (UTFPR / DAFIS), Rua Sete de Setembro 3165, CEP 80230-901 Curitiba, PR, Brazil

Accepted 2016 July 14. Received 2016 July 13; in original form 2016 June 2

ABSTRACT

Gomes-Júnior et al. published 3613 positions for the eight largest irregular satellites of Jupiter and 1787 positions for the largest irregular satellite of Saturn, Phoebe. These observations were made between 1995 and 2014 and have an estimated error of about 60–80 mas. Based on this set of positions, we derived new orbits for the eight largest irregular satellites of Jupiter: Himalia, Elara, Pasiphae, Carme, Lysithea, Sinope, Ananke and Leda. For Phoebe we updated the ephemeris from Desmars et al. using 75 per cent more positions than the previous one. Because of their orbital characteristics, it is common belief that the irregular satellites were captured by the giant planets in the early Solar system, but there is no consensus for a single model explaining where they were formed. Size, shape, albedo and composition would help to trace back their true origin, but these physical parameters are yet poorly known for irregular satellites. The observation of stellar occultations would allow for the determination of such parameters. Indeed Jupiter will cross the galactic plane in 2019–2020 and Saturn in 2018, improving a lot the chances of observing such events in the near future. Using the derived ephemerides and the UCAC4 catalogue we managed to identify 5442 candidate stellar occultations between 2016 January and 2020 December for the nine satellites studied here. We discussed how the successful observation of a stellar occultation by these objects is possible and present some potential occultations.

Key words: ephemerides – occultations – planets and satellites: general – planets and satellites: individual: Jovian and Saturnian irregular satellites.

1 INTRODUCTION

Irregular satellites revolve around giant planets at large distances in eccentric, highly inclined and frequently retrograde orbits. Because of these peculiar orbits, it is largely accepted that these objects did not form by accretion around their planet, but were captured in the early Solar system (Sheppard 2006).

There is no consensus for a single model explaining where the irregular satellites were formed. Ćuk & Burns (2004) showed that the progenitor of the Himalia group may have originated in heliocentric orbits similar to the Hilda asteroid group. Sheppard (2006) stated that the irregular satellites may be some of the objects that were formed within the giant planets region.

Grav et al. (2003) and Grav & Bauer (2007) showed that the irregular satellites from the giant planets have their colours and spectral slopes similar to C-, D- and P-type asteroids, Centaurs and trans-neptunian objects (TNOs). This suggests that they may have come from different locations in the early Solar system.

Sheppard (2006) and Jewitt & Haghighipour (2007) also explored the possibility that the irregular satellites originated as comets or TNOs. TNOs are highly interesting objects that, due to their large heliocentric distances, may be highly preserved with physical properties similar to those they had when they were formed (Barucci,

★E-mail: altair08@astro.ufrj.br
† Affiliated researcher at Observatoire de Paris/IMCCE, 77 Avenue Denfert Rochereau, 75014 Paris, France.

Table 1. Estimated diameter of the satellites and correspondent apparent diameter.

Satellite	Diameter of the satellites mas[a]	km	Ref.
Ananke	8	29	1
Carme	13	46	1
Elara	24	86	1
Himalia	41	$(150 \times 120) \pm 20^b$	2
Leda	5	20	1
Lysithea	10	36	1
Pasiphae	17	62	1
Sinope	10	37	1
Phoebe	32	212 ± 1.4^b	3

Notes. References: 1 – Rettig, Walsh & Consolmagno (2001); 2 – Porco et al. (2003); 3 – Thomas (2010).
[a]Using a mean distance from Jupiter of 5 au, from Saturn of 9 au and from Neptune of 30 au.
[b]From Cassini observations.

Brown & Emery 2008). This is even more true for the smaller objects, since in principle larger sizes favour physical differentiation processes in the body and vice versa. However, due to the distance, the smaller TNOs from this region are more difficult to observe. Thus, if irregular satellites – or at least a few of them – do share a common origin with small TNOs, and since these objects are situated at much closer heliocentric distances now, this gives a unique chance of observing and studying representatives of this specific TNO population in much greater detail than could ever be possible by direct observation of this population in the Kuiper Belt.

Phoebe is the most studied irregular satellite. Clark et al. (2005) suggest that its surface is probably covered by material of cometary origin. It was also stated by Johnson & Lunine (2005) that if the porosity of Phoebe is 15 per cent, Phoebe would have an uncompressed density similar to those of Pluto and Triton.

Gomes-Júnior et al. (2015, hereafter G15) obtained 6523 suitable positions for 18 irregular satellites between 1992 and 2014 with an estimated error in the positions of about 60–80 mas. For some satellites the number of positions obtained is comparable to the number used in the numerical integration of orbits by the JPL (Jacobson et al. 2012). They pointed out that the ephemeris of the irregular satellites has systematic errors that may reach 200 mas for some satellites.

We present in this paper new numerical integration of the orbits of the eight major irregular satellites of Jupiter (Himalia, Elara, Pasiphae, Lysithea, Carme, Ananke, Sinope and Leda) using only the positions obtained by G15 (see Section 2). For Phoebe, we updated the ephemeris of Desmars et al. (2013a) using the observations of G15, Peng et al. (2015), observations from Minor Planet Center and observations from Flagstaff.

Phoebe, being the most studied object with a good measured size, can be used to calibrate and evaluate the technique for similar objects. Up to date, no observation of a stellar occultation by an irregular satellite was published. Since their estimated sizes are very small (see Table 1), this may have discouraged earlier tries. But, in fact, given their relatively closer distances as compared to TNOs and Centaurs, and considering the precision of our ephemeris and of star positions, we can now reliably predict the exact location and instant where the shadow of the occultation will cross the Earth.

In Section 2, we present the new determination of the orbits. In Section 3, we present the predictions of the stellar occultations by irregular satellites, including some tests made to check the accuracy of the predictions. The final discussion is presented in Section 4.

2 ORBIT COMPUTATIONS

GJ15 published 3613 precise positions for the eight largest irregular satellites of Jupiter from observations made at the Observatório do Pico dos Dias (OPD), Observatoire Haute-Provence (OHP) and European Southern Observatory (ESO) between 1995 and 2014.

Here we compute new orbits based on the observations published in G15. First, because the reduction was made with a consistent and precise stellar catalogue and with a robust astrometry (PRAIA; Assafin et al. 2011). Second, besides recent observations, this consistent set of numerous and precise positions covers many orbital periods at many distinct orbital plane sights, allowing to fully constrain the orbit for the short time span explored in this work. For these reasons, only this set of positions was used for the satellites of Jupiter.

Because of the context of this work regarding to stellar occultations, the orbit fitting procedures used aimed primarily to derive precise ephemerides for the near future. Technically, the procedures easily allow for the continuous addition of more observations (old, new) aiming at refining the orbit fits.

2.1 Special-tailored ephemerides for Jupiter irregular satellites

The last observations used to develop current JPL ephemeris of the irregular satellites of Jupiter were obtained in 2012 (Jacobson et al. 2012). As a result, the errors in the JPL ephemeris for the current epoch may be probably too large to prevent accurate predictions of stellar occultations without any corrections.

Our numerical model describes the dynamical evolution of the irregular satellites of Jupiter in a jovicentric reference frame. The satellites are submitted to the influence of the Sun and the main bodies of the Solar system (from Mercury to Pluto, plus the Moon), as well as those of the Galilean satellites and the first harmonics of Jupiter's gravity field. The axes of the reference frame are expected to be those of the ICRS.

We use the following notations:

(i) in one dynamical family consisting of $\mathcal{N}$ irregular satellites, i will stand for the one whose equation of motion we are considering, l will stand for another irregular satellite in gravitational interaction belonging to the same family;
(ii) J Jupiter;
(iii) j another body of the Solar system, among the Galilean satellites, the Sun, the planets, Pluto and the Moon (14 bodies);
(iv) M_j the mass of the jth body, not an irregular satellite;
(v) m_i the mass of the irregular satellite i;
(vi) $\boldsymbol{r}_i$ the position of the ith body with respect to the centre of Jupiter; Q8
(vii) r_{ij} the distance between bodies i and j;
(viii) R_J the radius of Jupiter;
(ix) J_n the dynamic polar oblateness of the nth order for Jupiter's gravity field;
(x) $U_{\tilde{l}\hat{J}}$ potential generated by the oblateness of Jupiter on the satellite l;
(xi) Φ_i is the latitude of the ith satellite with respect to Jupiter's equator.

For an irregular satellite i, under the gravitational influence of Jupiter, the seven other irregular satellites, the regular Jovian

Table 2. Initial osculating elements for Jupiter irregular satellites at JD 245 1545.0 with respect to the centre of Jupiter.

Satellite	N	Time span	a (km)	e	I°	Ω°	ω°	v°
Himalia	1234	1995–2014	11372100 ± 500	0.166 ± 0.002	45.14 ± 0.15	39.77 ± 0.19	351.48 ± 0.46	97.35 ± 0.48
Elara	636	1996–2014	11741170 ± 690	0.222 ± 0.002	28.64 ± 0.18	68.42 ± 0.43	179.82 ± 0.56	339.08 ± 0.82
Lysithea	234	1996–2010	11739900 ± 1300	0.136 ± 0.004	51.12 ± 0.27	5.53 ± 0.52	53.0 ± 1.5	318.9 ± 2.0
Leda	98	1996–2009	11140300 ± 4300	0.173 ± 0.007	16.15 ± 0.75	272.6 ± 1.7	212.2 ± 3.6	218.8 ± 3.2
Pasiphae	609	1996–2013	23425000 ± 5000	0.379 ± 0.001	152.44 ± 0.10	284.59 ± 0.21	135.96 ± 0.19	236.97 ± 0.16
Sinope	221	1996–2009	22968800 ± 5200	0.316 ± 0.002	157.76 ± 0.12	256.62 ± 0.55	298.38 ± 0.55	167.57 ± 0.19
Carme	331	1996–2013	24202924 ± 4800	0.242 ± 0.001	147.13 ± 0.10	154.01 ± 0.25	47.90 ± 0.29	234.41 ± 0.19
Ananke	250	1996–2010	21683800 ± 7200	0.380 ± 0.002	172.29 ± 0.20	56.9 ± 1.2	123.3 ± 1.2	231.24 ± 0.21

Notes: N: number of observations used; a: semimajor axis; e: eccentricity; I: inclination relative to the equatorial reference plane J2000; Ω: longitude of the ascending node; ω: argument of periapsis; v: true anomaly.

satellites and the main bodies of the Solar system, the equation of motion is

$$\ddot{\boldsymbol{r}}_i = -GM_J\frac{\boldsymbol{r}_J-\boldsymbol{r}_i}{r_{iJ}^3} - \sum_{l=1,l\neq i}^{\mathcal{N}} Gm_l\frac{\boldsymbol{r}_l-\boldsymbol{r}_i}{r_{il}^3}$$
$$-\sum_{j=1}^{14} GM_j\left(\frac{\boldsymbol{r}_j-\boldsymbol{r}_i}{r_{ij}^3} - \frac{\boldsymbol{r}_j-\boldsymbol{r}_J}{r_{Jj}^3}\right)$$
$$+GM_J\nabla U_{\tilde{i}\hat{J}} - \sum_{l=1}^{\mathcal{N}} Gm_l\nabla U_{\tilde{l}\hat{J}}, \qquad (1)$$

where the last term in brackets and the last term in equation (1) represent undirect perturbations. The oblateness potential seen by a satellite i because of Jupiter is (with a similar expression for the oblateness seen by a satellite l)

$$U_{\tilde{i}\hat{J}} = -\frac{R_J^2J_2}{r_{iJ}^3}\left(\frac{3}{2}\sin^2\Phi_i - \frac{1}{2}\right)$$
$$-\frac{R_J^4J_4}{r_{iJ}^5}\left(\frac{35}{8}\sin^4\Phi_i - \frac{15}{4}\sin^2\Phi_i + \frac{3}{8}\right)$$
$$-\frac{R_J^6J_6}{r_{iJ}^7}\left(\frac{231}{16}\sin^6\Phi_i - \frac{315}{16}\sin^4\Phi_i + \frac{105}{16}\sin^2\Phi_i - \frac{5}{16}\right). \qquad (2)$$

The expressions of ∇U have been developed in Lainey, Duriez & Vienne (2004). The equations of motion are integrated with the 15th order numerical integrator RADAU (Everhart 1985) using a constant step of one day. The positions of the objects of the Solar system are provided by the DE423 ephemeris (Folkner 2010), while those of the Galilean satellites are provided by NOE2010 (Lainey et al. 2004). Our model was fitted to the observations through a least-squares procedure. The satellites were integrated one dynamical family at a time, to gain computing time, while losing minimum precision. Indeed, the interactions between satellites not belonging to the same dynamical family are negligible considering the short time span of our integration.

The obtained ephemeris is hereafter referred to as STE, for special-tailored ephemeris. The initial osculating elements at the origin of integration, the number and time span of the observations of each satellite are presented in Table 2.

Some methods to derive the errors of the ephemeris of irregular satellites can be found in Emelyanov (2010). In the Natural Satellites Ephemeride Server MULTI-SAT (Emelyanov & Arlot 2008) the precisions can be obtained for the satellites at any given time from the Emelyanov (2005) ephemeris updated to 2012 February 19. However, since the practical realization of the STE ephemeris is for

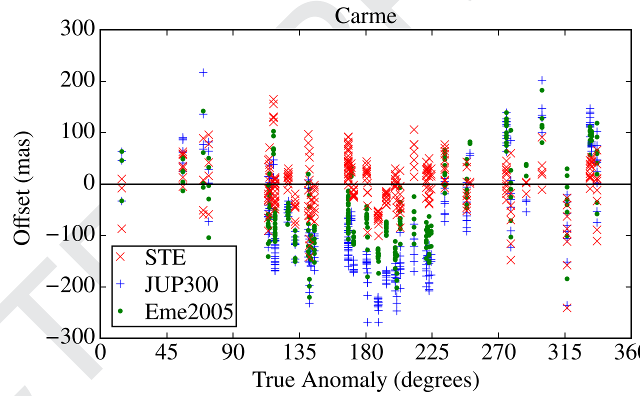

Figure 1. Offsets in declination of the positions published by G15 for Carme. The red ‘x’ relate to the STE (rms = 51), the blue ‘+’ to the jup300 JPL ephemeris (rms = 130) and the green dot to Emelyanov (2005) (rms = 92). As expected, the ephemeris offsets pointed out by G15 are reduced with the STE ephemeris.

help improving the prediction of stellar occultations by the irregular satellites in the immediate future, it is interesting to compare the STE with the other relevant ephemerides for the next few years.

We compared the STE ephemeris to the JPL for all the Jupiter satellites we fitted, until 2021. For instance, the maximum difference between 2015 and 2021 is at most 98 mas in $\Delta\alpha\cos\delta$ and 58 mas in $\Delta\delta$ for Himalia and 181 mas in $\Delta\alpha\cos\delta$ and 152 mas in $\Delta\delta$ for Carme.

Fig. 1 displays the offsets of the positions published by G15 for the satellite Carme in declination relative to the STE ephemeris, to Jacobson et al. (2012) jup300 JPL ephemeris and Emelyanov (2005)[1] ephemeris. The DE431 planetary ephemeris (Folkner et al. 2014) was used to calculate the positions of Jupiter for the three models. We see that the systematic JPL ephemeris offsets pointed out by G15 are reduced with our ephemeris, as expected. Q10

In Table 3 we present the mean offsets and the respective standard deviation of the G15 positions relative to the same three ephemeris as above. We can see that the mean offsets as well as most of their standard deviations are greatly reduced with the STE ephemeris. Of course, by construction, we should expect smaller offsets in the comparison of G15 positions with STE. However, it is not obvious that these offsets should be that smaller in comparison with the other ephemeris offsets. Notice that the G15 positions come from observations made with very distinct instruments at distant sites located at both Earth hemispheres (good parallax angle coverage),

[1] Last update: 2012 February 19.

Table 3. Mean offsets and standard deviation of the G15 positions relative to the STE, Jacobson et al. (2012) and Emelyanov (2005) ephemeris.

	STE		JPL		Eme2008	
Satellite	$\Delta\alpha\cos\delta$ (mas)	$\Delta\delta$ (mas)	$\Delta\alpha\cos\delta$ (mas)	$\Delta\delta$ (mas)	$\Delta\alpha\cos\delta$ (mas)	$\Delta\delta$ (mas)
Himalia	−15 ± 66	−7 ± 54	−19 ± 80	−11 ± 52	−18 ± 72	−13 ± 53
Elara	3 ± 92	−12 ± 57	20 ± 92	−50 ± 69	23 ± 94	−83 ± 81
Lysithea	15 ± 79	−21 ± 68	40 ± 92	−43 ± 77	117 ± 193	−76 ± 185
Leda	−9 ± 67	−8 ± 77	60 ± 117	−13 ± 95	166 ± 162	92 ± 95
Pasiphae	4 ± 89	−16 ± 57	−17 ± 130	−82 ± 85	−10 ± 102	−54 ± 74
Sinope	9 ± 79	−4 ± 47	10 ± 228	−35 ± 76	11 ± 227	−52 ± 63
Carme	14 ± 73	−1 ± 51	−3 ± 114	−80 ± 102	−6 ± 108	−45 ± 80
Ananke	−10 ± 90	3 ± 73	60 ± 127	−108 ± 99	101 ± 180	−107 ± 120

making this set of positions not remarkably distinct than any set of positions that were used in the construction of the other two ephemeris. Thus, these ephemeris offsets comparisons suggest that the accuracy of the STE ephemeris is at least slightly better than that of the other ephemeris, at least for the time span of our satellites' observations. This supports the utility of the STE ephemeris for the next few years, making it one of the best choices to use in stellar occultation predictions in the short future for these satellites.

2.2 Phoebe's ephemeris

For the specific case of Phoebe, the ninth satellite of Saturn, we have updated the ephemeris published in Desmars et al. (2013a). The new ephemeris (PH15) used the same dynamical model, including the perturbations of the Sun and the eight planets, the eight major satellites of Saturn and the J_2 parameter. The observations used to fit the model are identical to Desmars et al. (2013a) (including 223 Cassini observations) with additional observations from G15, Peng et al. (2015), observations from Minor Planet Circulars between 2012 and 2014 (available on the Natural Satellite Data Center Arlot & Emelyanov 2009), and observations from Flagstaff (U.S.N.O 2015) between 2012 and 2014. It represents a total number of 5886 observations from 1898 to 2014. In contrast, in Desmars et al. (2013a) were used 3367 observations from 1898 to 2012. This represents an increase of almost 75 per cent in the number of observations, mainly with recent observations which is required for our purpose.

In Fig. 2 we compare our ephemeris (PH15) with the sat375 JPL[2] ephemeris. The difference between them is smaller than 30 mas (<10 mas in declination.). This difference is smaller than the apparent diameter of Phoebe (see Table 1).

We computed the precision of the PH15 ephemeris considering three sets of observations: all the positions available; only the positions of G15; and all the positions without G15. The precision is computed by propagation of the covariance matrix of the orbit determination process and by linear transformations giving the covariance matrix in spherical coordinates (right ascension and declination) at a specific date (for more details, see Desmars et al. 2013b). This last matrix then provides the standard deviation in right ascension σ_α and declination σ_δ at the required date, with $\sigma_s = \sqrt{\sigma_\alpha^2 \cos^2\delta + \sigma_\delta^2}$ being the total error in the celestial sphere.

In Fig. 3 we show the comparison between them for the time span 2016–2021 in on-sky Phoebe–Saturn angular separation. It is

[2] Jacobson, RA 2015 February 27. 'Satellite Ephemeris: sat375', JPL Satellite Ephemeris File Release, ftp://ssd.jpl.nasa.gov/pub/eph/satellites/nio/LINUX_PC/sat375l.txt

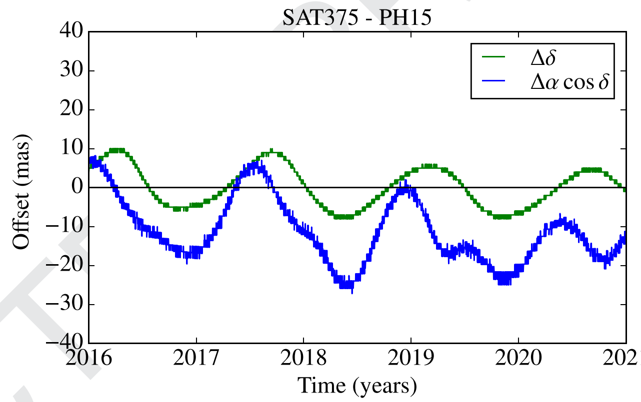

Figure 2. Comparison between the PH15 and sat375 JPL ephemeris for the satellite Phoebe.

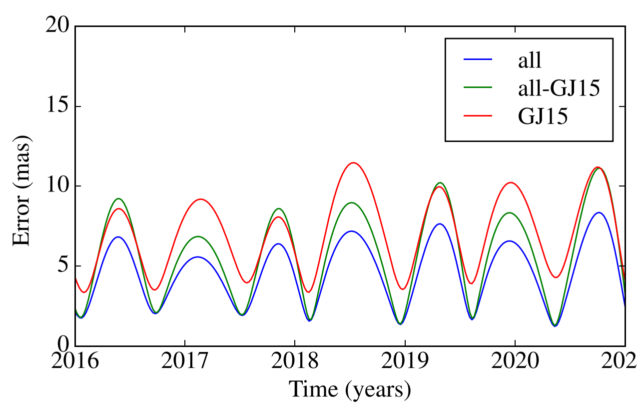

Figure 3. Comparison of the precision in on-sky Phoebe–Saturn angular separation for the PH15 ephemeris where three different sets of positions were used to compute the ephemeris: all observations; only positions of G15; and all the positions without G15.

possible to see that even considering only the positions of G15, the estimated error of the ephemeris is smaller than 12 mas. The computed precision does not take into account the precision in the position of Saturn.

3 PREDICTION OF STELLAR OCCULTATIONS

3.1 Candidate events

The prediction of the occultations was made by crossing the stellar coordinates and proper motions of the UCAC4 catalogue (Zacharias et al. 2013) with the ephemeris presented in Section 2. The search

Table 4. Number of stellar occultations for each satellite from 2016 January up to 2020 December.

Satellite	2016	2017	2018	2019	2020	Total
Ananke	12	16	49	359	187	623
Carme	20	14	30	369	220	653
Elara	14	16	33	305	193	561
Himalia	15	12	54	257	230	568
Leda	8	24	38	362	208	640
Lysithea	16	11	35	330	212	604
Pasiphae	20	19	44	362	206	651
Sinope	15	21	34	356	256	682
Phoebe	32	98	238	79	13	460

for stellar candidates follows the same procedure as presented by Assafin et al. (2010, 2012) and Camargo et al. (2014).

We predicted occultations for the eight major irregular satellites of Jupiter, Ananke, Carme, Elara, Himalia, Leda, Lysithea, Pasiphae and Sinope, and for Phoebe of Saturn.

A total of 5442 events were identified between 2016 January and 2020 December. In Table 4 we present the number of stellar occultations predicted by year for each satellite. It is possible to see an increase in the number of events found for Phoebe in 2018 and for the satellites of Jupiter in 2019–2020. This is because at that periods these satellites will cross the apparent galactic plane. We call attention that about 10 per cent of the events will involve stars brighter than magnitude $R = 14$ (and almost 25 per cent brighter than $R = 15$), which helps the attempt of amateur observers.

Table 5 shows a sample of the catalogue of predicted occultations and their parameters, which are necessary to produce occultation maps. Since these objects are very small, the duration of each event is a few seconds. All the occultation tables and maps will be publicly available at the Centre de Données astronomiques de Strasbourg (CDS). In Fig. 4 we show an example of an occultation map. This is an occultation by Elara that will happen in 2017 February 21. This event can be observed from Australia and it is one of the best opportunities for this object due to the slow velocity of the event and it involves a bright star ($R^* = 12.4$).

The first preliminary catalogue version of the ESA astrometry satellite *GAIA* (de Bruijne 2012) is expected to be released up to the end of 2016 (the catalogue with five-parameter astrometric solutions is up to the end of 2017). The precise star positions to be derived by *GAIA* will provide better predictions with the main source of error being the ephemeris. Astrometric reduction of observations published in G15 will be revised with the *GAIA* catalogue and the predictions will be improved. In that context, in the *GAIA* era, the occultations predicted will be updated.

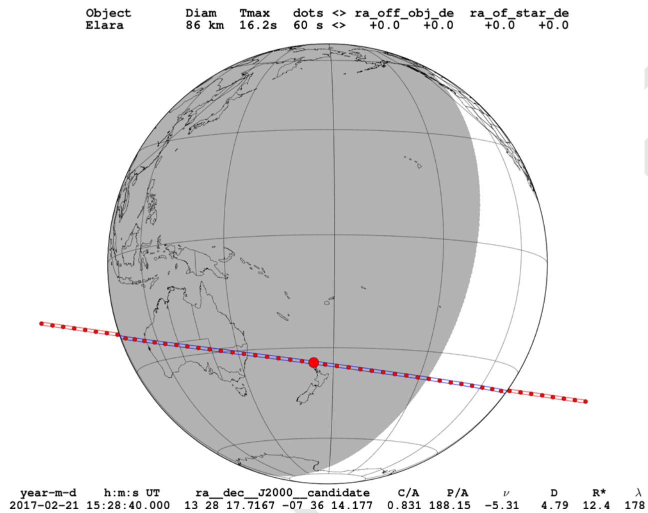

Figure 4. Occultation map for Elara. The central red dot shows the geocentric closest approach of the shadow. The small ones show the centre of the shadow separated by 60s. The lines show the path of the shadow over the Earth. The shadow moves from right to left. Labels: Diam: diameter of the object; Tmax: maximum duration of the event for an observation in the centre of the shadow; C/A: apparent geocentric distance between the satellite and the star (also known as the apparent distance in the plane of the sky between the shadow and the centre of the Earth) at the moment of the geocentric closest approach, in arcseconds; P/A: the satellite position angle with respect to the occulted star at C/A, in degrees; ν: relative velocity of event in km s^{-1}; D: geocentric distance to the occulting object in au; R^*: normalized UCAC4 magnitude in the R band to a common shadow velocity of 20 km s^{-1}; λ: east longitude of subplanet point in degrees, positive towards east, at the central instant of the geocentric closest approach (see the notes of Table 5).

Table 5. A sample of stellar occultation predictions for Pasiphae.

dd mm yyyy h:m:s	RA (ICRS) Dec.	C/A	P/A	ν	D	R^*	λ	LST	$\mu_{\alpha\star}$	μ_δ
09 04 2016 03:58:19	11 14 36.7707 +07 39 20.7610	1.003	17.9	-12.88	4.54	14.9	271.	22:03	12.	-33.
13 06 2016 00:16:12	11 12 48.5020 +07 06 43.3520	0.661	30.0	+14.32	5.50	13.9	262.	17:45	-1.	1.
27 06 2016 13:56:09	11 18 03.4160 +06 23 45.1940	1.707	28.0	+20.29	5.74	11.7	44.	16:53	4.	-10.
18 07 2016 15:07:24	11 28 15.5076 +05 05 31.8060	0.942	26.7	+27.80	6.05	14.0	8.	15:40	4.	4.
22 07 2016 16:15:07	11 30 30.4310 +04 48 43.4340	0.644	206.5	+29.04	6.11	14.6	348.	15:27	23.	-24.
24 07 2016 01:37:34	11 31 17.8471 +04 42 49.0540	0.029	206.6	+29.46	6.12	15.1	206.	15:22	2.	-8.
24 07 2016 17:37:18	11 31 40.7472 +04 39 57.5060	0.840	26.5	+29.66	6.13	14.9	326.	15:20	-11.	-1.

Notes. Entries included: day of the year and UTC central instant of the prediction; right ascension and declination of the occulted star – at the central instant of the occultation (corrected by proper motions); C/A: apparent geocentric distance between the satellite and the star (also known as the distance between the shadow and the centre of the Earth) at the moment of the geocentric closest approach, in arcseconds; P/A: the satellite position angle with respect to the occulted star at C/A, in degrees (zero at north of the star, increasing clockwise); ν: relative velocity of event in km s^{-1}; positive = prograde, negative = retrograde; D: geocentric distance to the occulting object in au; R^*: normalized UCAC4 magnitude in the R band to a common shadow velocity of 20 km s^{-1} by the relationship $R^* = R_{UCAC4} + 2.5 \times \log 10\left(\frac{\text{velocity}}{20\,\text{km}\,\text{s}^{-1}}\right)$, the value 20 km s^{-1} is typical of events around the opposition; λ: east longitude of subplanet point in degrees, positive towards east, at the instant of the geocentric closest approach; LST: UT + λ: local solar time at subplanet point, hh:mm; $\mu_{\alpha\star}$ and μ_δ: proper motions in right ascension and declination, respectively (mas yr^{-1}). For more detailed information about the definition and use of these stellar occultation geometric elements see Assafin et al. (2010).

3.2 Robustness of predictions

Since 2009 many successful observations of stellar occultations by TNOs have been reported in the literature (Elliot et al. 2010; Sicardy et al. 2011; Ortiz et al. 2012; Braga-Ribas et al. 2013), the main disadvantages in their prediction being large heliocentric distances and ephemeris error, facts somewhat compensated for the larger diameters involved. In contrast to TNOs, the irregular satellites have much better ephemeris because the orbits of their host planets are better known, their observational time span is much wider and covers many orbital periods. Moreover, the irregular satellites are much closer to Earth which implies in a much smaller shadow path error in kilometres. These advantages may be somewhat balanced by the smaller sizes estimated for the irregular satellites. Thus, in comparison, the chances for a successful observation of a stellar occultation by an irregular satellite should be considered at least also as good as those by TNOs.

Observing a stellar occultation demands a great effort. And, in our case, the shadow covers a very restricted area on the Earth because of the size of the irregular satellites. Since no stellar occultation by an irregular satellite was observed up to date, and since we want to be sure that we can start observational campaigns with reasonable chances of success, we tested the robustness of an occultation prediction for a large target.

The test design consisted in observing the object and star to be occulted near the date of the event predicted when the two objects were present in the same field of view (FOV), close to each other. Thus, the relative positions between the two objects had minimal influence of the errors of the reference catalogue of stars used and possible field distortions (Peng et al. 2008, and references therein). The relative positions of the star and satellite were used to check the original prediction. Notice that in the test we did not attempt to observe any actual occultation. The test could be performed at any site, regardless of the Earth location where the occultation would in fact be visible.

We tested the occultation by Himalia predicted to occur on 2015 March 3. The shadow would cross the northern part of South America. For the event, four situations were considered.

(i) Our nominal, published prediction with the STE ephemeris (see Section 2), and the nominal UCAC4 position of the star.

(ii) Prediction with the JPL ephemeris and the nominal UCAC4 position of the star.

(iii) Prediction from star and satellite offsets calculated from observations made a few days before the occultation when the objects were very separated (different FOVs).

(iv) Same as (iii) but with the star and the satellite close in the same FOV.

Table 6 shows the differences between the predictions in the four situations. For situation (iii) we observed the objects on February 22 with the Zeiss telescope (diameter = 0.6 m; FOV = 12.6 arcmin; pixel scale = 0.37 arcsec pixel^{-1}) at the Observatório do Pico dos Dias, Brazil (OPD, IAU code 874, 45°34′57″W, 22°32′04″S, 1864 m). On that day, Himalia and the star were observed in separate FOVs as they were still far apart. On the night of the event, March 3, the objects were observed with Perkin-Elmer telescope (diameter = 1.6 m; FOV = 5.8 arcmin; pixel scale = 0.17 arcsec pixel^{-1}) at OPD just over an hour after the time scheduled for the event. Satellite and star were separated by about 16 arcsec, so very close to each other (situation (iv)). From the calculated offsets, the centre of the shadow was obtained. Notice that the shadow path was not predicted to cross the OPD (which was located at almost 2000 km south from the shadow path). This was not necessary for testing the prediction.

Table 6. Comparison between the predictions of the Himalia occultation at 2015 March 3.

	Differences with respect to the STE prediction		
Method	Instant of C/A	C/A	Sit.
STE	00:39:51 UTC	0″.703	(i)
JPL	−26 s	+11 mas (36 km)	(ii)
Feb. 22 Obs.	−14 s	−20 mas (65 km)	(iii)
Mar. 3 Obs.	−36 s	−09 mas (29 km)	(iv)

Notes. C/A: geocentric closest approach; Sit: situation test considered.

The critical parameter in the comparisons is the C/A, which here is related to latitudes. The apparent radius of Himalia is about 20 mas (see Table 1). In the context of the test, for a 0 mas offset in C/A we would have 100 per cent probability of observing the occultation, and 0 per cent in the case of a C/A offset equal to or larger than 20 mas, the radius of Himalia. From Table 6, we have nearly 0 per cent probability of success in situation (iii), for which the offset in C/A was −20 mas, but when the relative astrometry was poor, 10 d prior to the event. Once at the day of the event in situation (iv), the C/A offset dropped to −9 mas only, corresponding to a 55 per cent probability of success. Comparison with the prediction using the JPL ephemeris (situation (ii)) gives a +11 mas C/A offset, or a compatibility of 45 per cent between the ephemerides. All this suggests that there was a good probability of observing the event. The largest differences between the shadows of the four situations were 36 s in time along the shadow path and 101 km (31 mas) in the direction perpendicular to the shadows, suggesting that observers should be spread in narrow latitude ranges 100 km wide.

4 DISCUSSION

We performed new numerical integrations for improving the orbits of some of the larger irregular satellites. Consequently, with our ephemeris, we predicted stellar occultations aiming to access fundamental parameters like size, shape, albedo, ultimately aiming to track the formation origin of these bodies.

For the irregular satellites of Jupiter (Ananke, Carme, Elara, Himalia, Leda, Lysithea, Pasiphae and Sinope), we produced ephemeris using only the observations of G15. These new ephemerides are denominated STE.

We also updated the ephemeris of Phoebe (Desmars et al. 2013a) using the observations of G15, Peng et al. (2015), observations from MPC and from Flagstaff. A total of 5886 observations between 1989 and 2014 were used in the process. This represents an increase of about 75 per cent in the number used to generate the ephemeris of Phoebe in Desmars et al. (2013a).

As it was shown for Phoebe, when we use only the positions of G15, the ephemeris presents a precision in the order of those where all the positions were used. Moreover, the case of Phoebe is particular because we have many observations in a large time spam (1898–2014) including observations from Cassini. For the Jovian satellites with fewer observations, the precision we have by using only G15 observations may be quite equivalent or even better than the precision of other ephemeris for the short time span explored in this work.

We predict stellar occultations for the period of 2016–2020 for eight irregular satellites of Jupiter: Ananke, Carme, Elara, Himalia, Leda, Lysithea, Pasiphae, and Sinope; and one satellite of Saturn:

Phoebe. The procedure used was the same as that for the prediction of stellar occultations by Pluto and its satellites in Assafin et al. (2010) and by Centaurs and TNOs in Assafin et al. (2012) and Camargo et al. (2014). The candidate stars were searched in the UCAC4 catalogue. The occasional passage of Jupiter by the galactic plane in 2019–2020 and Saturn in 2018 creates the best opportunity of observing stellar occultations in the near future due to the great density of stars in the region. Indeed, a total of 5442 events are foreseen. The next time that Jupiter will cross the central side of the galactic plane will be in 2031 and Saturn in 2046–2047.

In a broader, general sense, the probability of successfully observing an occultation is roughly the ratio of the satellite's radius by the budget error (2σ for a 95 per cent confidence level) of ephemeris and star position. Thus, UCAC4 errors ranging between 20 and 50 mas (1σ) combined with a mean error (1σ) in the JPL ephemeris of 30 mas for Himalia and 150 mas for Leda published in table 2 of Jacobson et al. (2012) would give 28–17 per cent probability of observing such an event by Himalia and $\approx$2 per cent for Leda, the smallest irregular satellite in the sample. Observations a few days before the date of occultation predicted may improve the combined errors to 40–80 mas, depending on the magnitude of the objects. This probability is estimated for a single observing site, and we expect to reach higher probability with multisites.

The test made with an occultation expected to happen in 2015 March 3 for Himalia showed that this event would probably have been observed successfully in case there were observers available in the shadow area. The results show satisfying small offsets with respect to the local of the prediction.

GJ15 also observed Sycorax (satellite of Uranus) and Nereid (satellite of Neptune). There were few observations of Sycorax distributed in 9 nights over 2 yr which did not cover one orbital period. For Nereid, the observations covered many orbital periods, but due to Nereid's large orbital eccentricity there are no observations near the pericentre.

Uranus and Neptune are crossing a very low dense region of stars. This results in almost no stellar occultation by these objects up to 2020. In fact, using JPL ephemeris, we identified only two events for each satellite in this period, but due to the bad conditions of the events (shadow far from observatories; faint stars) we chose not to publish any events here. For these reasons we did not attempt to generate new orbits for these satellites here.

Continuous observations of the satellites are recommended and fitting of our dynamical model to those observations are expected to reduce the respective STE ephemeris errors. The first version of the *GAIA* catalogue is to be released up to the end of 2016 and will improve the position error of the stars to the 1–5 mas level. Re-reduction of older positions, and reduction of new positions of irregular satellites with *GAIA* will improve new orbit determinations. It will also allow for the discovery of occultations by more stars not present in the UCAC4 catalogue. The release of the *GAIA* catalogue should have a positive impact on both the astrometric precision of occulted stars and the reduction of new astrometric positions of the satellites. As a result, prediction of stellar occultations by irregular satellites shall increase in number as well as in precision and success.

ACKNOWLEDGEMENTS

ARG-J thanks the financial support of CAPES. MA thanks the CNPq (Grants 473002/2013-2 and 308721/2011-0) and FAPERJ (Grant E-26/111.488/2013). RV-M thanks grants: CNPq-306885/2013, Capes/Cofecub-2506/2015, Faperj: PAPDRJ-45/2013 and Cient.Est-05/2015. JIBC acknowledges CNPq for a PQ2 fellowship (process number 308489/2013-6). BEM thanks the financial support of CAPES. FB-R acknowledges PAPDRJ-FAPERJ/CAPES E-43/2013 number 144997, E-26/101.375/2014. The numerical model of the satellites of Jupiter was developed during a post-doctoral contract funded by the Chinese Academy of Sciences (CAS) and supported by the National Scientific Fund of China (NSFC). The authors thank Dr Nikolay Emelyanov for his comments to improve the paper.

REFERENCES

Arlot J.-E., Emelyanov N. V., 2009, A&A, 503, 631
Assafin M., Camargo J. I. B., Vieira Martins R., Andrei A. H., Sicardy B., Young L., da Silva Neto D. N., Braga-Ribas F., 2010, A&A, 515, A32
Assafin M., Vieira Martins R., Camargo J. I. B., Andrei A. H., Da Silva Neto D. N., Braga-Ribas F., 2011, in Tanga P., Thuillot W., eds, Gaia FUN-SSO Workshop Proc., Gaia Follow-Up Network for the Solar System Objects. p. 85 Q11
Assafin M., Camargo J. I. B., Vieira Martins R., Braga-Ribas F., Sicardy B., Andrei A. H., da Silva Neto D. N., 2012, A&A, 541, A142
Barucci M. A., Brown M. E., Emery J. P., 2008, in Barucci M. A., Boehnhardt H., Cruikshank D. P., Morbidelli A., Dotson R., eds, Composition and Surface Properties of Transneptunian Objects and Centaurs. Univ. Arizona Press, Tuscan, AZ, p. 143
Braga-Ribas F. et al., 2013, ApJ, 773, 26
Camargo J. I. B. et al., 2014, A&A, 561, A37
Clark R. N. et al., 2005, Nature, 435, 66
Ćuk M., Burns J. A., 2004, Icarus, 167, 369
de Bruijne J. H. J., 2012, Ap&SS, 341, 31
Desmars J., Li S. N., Tajeddine R., Peng Q. Y., Tang Z. H., 2013a, A&A, 553, A36
Desmars J., Bancelin D., Hestroffer D., Thuillot W., 2013b, A&A, 554, A32
Elliot J. L. et al., 2010, Nature, 465, 897
Emelyanov N. V., 2005, A&A, 435, 1173
Emelyanov N., 2010, Planet. Space Sci., 58, 411
Emelyanov N. V., Arlot J.-E., 2008, A&A, 487, 759
Everhart E., 1985, in Carusi A., Valsecchi G. B., eds, Proc. IAU Colloq. 83, ASSL, Vol. 115, Dynamics of Comets: Their Origin and Evolution. Reidel, Dordrecht, p. 185
Folkner W. M., 2010. Technical Report, Jet Propulsion Laboratory Interoffice Memo. IOM 343R-10-001
Folkner W. M., Williams J. G., Boggs D. H., Park R. S., Kuchynka P., 2014, The Planetary and Lunar Ephemerides de430 and de431. Technical Report, Jet Propulsion Laboratory
Gomes-Júnior A. R. et al., 2015, A&A-PLX2 (GJ15) Q12
Grav T., Bauer J., 2007, Icarus, 191, 267
Grav T., Holman M. J., Gladman B. J., Aksnes K., 2003, Icarus, 166, 33
Jacobson R., Brozović M., Gladman B., Alexandersen M., Nicholson P. D., Veillet C., 2012, AJ, 144, 132
Jewitt D., Haghighipour N., 2007, ARA&A, 45, 261
Johnson T. V., Lunine J. I., 2005, Nature, 435, 69
Lainey V., Duriez L., Vienne A., 2004, A&A, 420, 1171
Ortiz J. L. et al., 2012, Nature, 491, 566
Peng Q., Vienne A., Lainey V., Noyelles B., 2008, Planet. Space Sci., 56, 1807
Peng Q. Y., Wang N., Vienne A., Zhang Q. F., Li Z., Meng X. H., 2015, MNRAS, 449, 2638
Porco C. C. et al., 2003, Science, 299, 1541
Rettig T., Walsh K., Consolmagno G., 2001, Icarus, 154, 313
Sheppard S. S., 2006, in Daniela L., Sylvio Ferraz M., Angel F. J., eds, Proc. IAU Symp. 229, Asteroids, Comets, Meteors. Cambridge Univ. Press, Cambridge, p. 319
Sicardy B. et al., 2011, Nature, 478, 493
Thomas P., 2010, Icarus, 208, 395

U.S.N.O, 2015, Flagstaff Astrometric Scanning Transit Telescope Planet and Planetary Satellite Observations. http://www.nofs.navy.mil/data/plansat.html

Zacharias N., Finch C. T., Girard T. M., Henden A., Bartlett J. L., Monet D. G., Zacharias M. I., 2013, AJ, 145, 44

SUPPORTING INFORMATION

Additional Supporting Information may be found in the online version of this article:

occ_tables.zip
(http://www.mnras.oxfordjournals.org/lookup/suppl/doi:10.1093/mnras/stw1738/-/DC1).

Please note: Oxford University Press is not responsible for the content or functionality of any supporting materials supplied by the authors. Any queries (other than missing material) should be directed to the corresponding author for the article.

This paper has been typeset from a TEX/LATEX file prepared by the author.

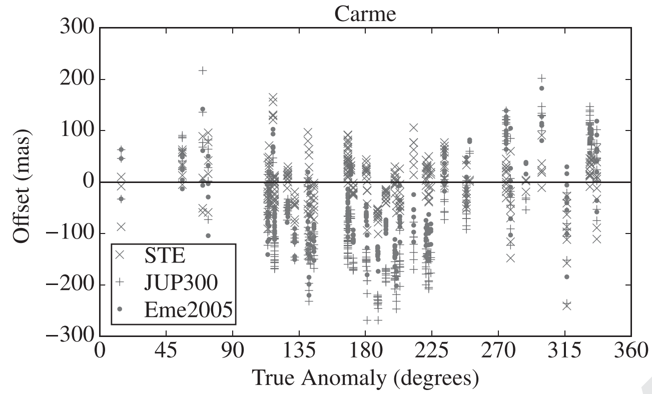

Figure 1. Offsets in declination of the positions published by G15 for Carme. The red 'x' relate to the STE (rms = 51), the blue '+' to the jup300 JPL ephemeris (rms = 130) and the green dot to Emelyanov (2005) (rms = 92). As expected, the ephemeris offsets pointed out by G15 are reduced with the STE ephemeris.

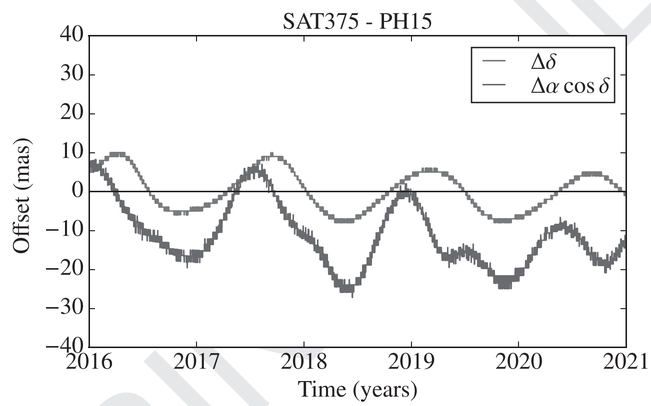

Figure 2. Comparison between the PH15 and sat375 JPL ephemeris for the satellite Phoebe.

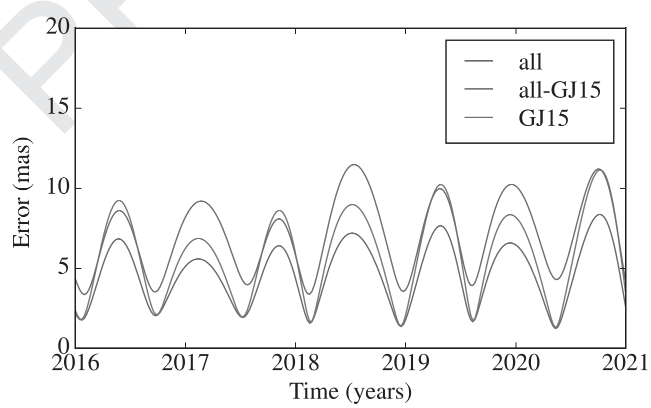

Figure 3. Comparison of the precision in on-sky Phoebe–Saturn angular separation for the PH15 ephemeris where three different sets of positions were used to compute the ephemeris: all observations; only positions of G15; and all the positions without G15.

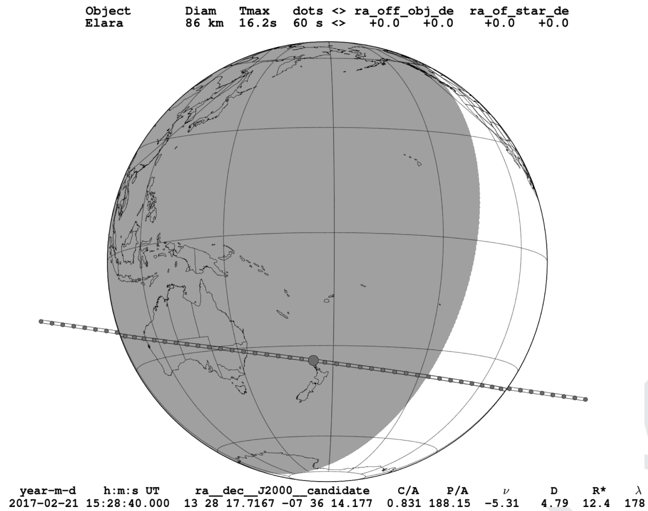

Figure 4. Occultation map for Elara. The central red dot shows the geocentric closest approach of the shadow. The small ones show the centre of the shadow separated by 60s. The lines show the path of the shadow over the Earth. The shadow moves from right to left. Labels: Diam: diameter of the object; Tmax: maximum duration of the event for an observation in the centre of the shadow; C/A: apparent geocentric distance between the satellite and the star (also known as the apparent distance in the plane of the sky between the shadow and the centre of the Earth) at the moment of the geocentric closest approach, in arcseconds; P/A: the satellite position angle with respect to the occulted star at C/A, in degrees; ν: relative velocity of event in km s^{-1}; D: geocentric distance to the occulting object in au; R^*: normalized UCAC4 magnitude in the R band to a common shadow velocity of 20 km s^{-1}; λ: east longitude of subplanet point in degrees, positive towards east, at the central instant of the geocentric closest approach (see the notes of Table 5).

List of astronomical key words (updated 2013 July)

This list is common to *Monthly Notices of the Royal Astronomical Society, Astronomy and Astrophysics*, and *The Astrophysical Journal*. In order to ease the search, the key words are subdivided into broad categories. No more than *six* subcategories altogether should be listed for a paper.

The subcategories in boldface containing the word 'individual' are intended for use with specific astronomical objects; these should never be used alone, but always in combination with the most common names for the astronomical objects in question. Note that each object counts as one subcategory within the allowed limit of six.

The parts of the key words in italics are for reference only and should be omitted when the key words are entered on the manuscript.

General

editorials, notices
errata, addenda
extraterrestrial intelligence
history and philosophy of astronomy
miscellaneous
obituaries, biographies
publications, bibliography
sociology of astronomy
standards

Physical data and processes

acceleration of particles
accretion, accretion discs
asteroseismology
astrobiology
astrochemistry
astroparticle physics
atomic data
atomic processes
black hole physics
chaos
conduction
convection
dense matter
diffusion
dynamo
elementary particles
equation of state
gravitation
gravitational lensing: strong
gravitational lensing: weak
gravitational lensing: micro
gravitational waves
hydrodynamics
instabilities
line: formation
line: identification
line: profiles
magnetic fields
magnetic reconnection
(magnetohydrodynamics) MHD
masers
molecular data
molecular processes
neutrinos
nuclear reactions, nucleosynthesis, abundances
opacity
plasmas
polarization
radiation: dynamics
radiation mechanisms:general
radiation mechanisms: non-thermal
radiation mechanisms: thermal
radiative transfer
relativistic processes
scattering
shock waves
solid state: refractory
solid state: volatile
turbulence
waves

Astronomical instrumentation, methods and techniques

atmospheric effects
balloons
instrumentation: adaptive optics
instrumentation: detectors
instrumentation: high angular resolution
instrumentation: interferometers
instrumentation: miscellaneous
instrumentation: photometers
instrumentation: polarimeters
instrumentation: spectrographs
light pollution
methods: analytical
methods: data analysis
methods: laboratory: atomic
methods: laboratory: molecular
methods: laboratory: solid state
methods: miscellaneous
methods: numerical
methods: observational
methods: statistical
site testing
space vehicles
space vehicles: instruments
techniques: high angular resolution
techniques: image processing
techniques: imaging spectroscopy
techniques: interferometric
techniques: miscellaneous
techniques: photometric
techniques: polarimetric
techniques: radar astronomy
techniques: radial velocities

techniques: spectroscopic
telescopes

Astronomical data bases

astronomical data bases: miscellaneous
atlases
catalogues
surveys
virtual observatory tools

Astrometry and celestial mechanics

astrometry
celestial mechanics
eclipses
ephemerides
occultations
parallaxes
proper motions
reference systems
time

The Sun

Sun: abundances
Sun: activity
Sun: atmosphere
Sun: chromosphere
Sun: corona
Sun: coronal mass ejections (CMEs)
Sun: evolution
Sun: faculae, plages
Sun: filaments, prominences
Sun: flares
Sun: fundamental parameters
Sun: general
Sun: granulation
Sun: helioseismology
Sun: heliosphere
Sun: infrared
Sun: interior
Sun: magnetic fields
Sun: oscillations
Sun: particle emission
Sun: photosphere
Sun: radio radiation
Sun: rotation
(Sun:) solar–terrestrial relations
(Sun:) solar wind
(Sun:) sunspots
Sun: transition region
Sun: UV radiation
Sun: X-rays, gamma-rays

Planetary systems

comets: general
comets: individual: . . .
Earth
interplanetary medium
Kuiper belt: general
Kuiper belt objects: individual: . . .
meteorites, meteors, meteoroids
minor planets, asteroids: general
minor planets, asteroids: individual: . . .
Moon
Oort Cloud
planets and satellites: atmospheres
planets and satellites: aurorae
planets and satellites: composition
planets and satellites: detection
planets and satellites: dynamical evolution and stability
planets and satellites: formation
planets and satellites: fundamental parameters
planets and satellites: gaseous planets
planets and satellites: general
planets and satellites: individual: . . .
planets and satellites: interiors
planets and satellites: magnetic fields
planets and satellites: oceans
planets and satellites: physical evolution
planets and satellites: rings
planets and satellites: surfaces
planets and satellites: tectonics
planets and satellites: terrestrial planets
planet–disc interactions`
planet–star interactions
protoplanetary discs
zodiacal dust

Stars

stars: abundances
stars: activity
stars: AGB and post-AGB
stars: atmospheres
(stars:) binaries *(including multiple)*: close
(stars:) binaries: eclipsing
(stars:) binaries: general
(stars:) binaries: spectroscopic
(stars:) binaries: symbiotic
(stars:) binaries: visual
stars: black holes
(stars:) blue stragglers
(stars:) brown dwarfs
stars: carbon
stars: chemically peculiar
stars: chromospheres
(stars:) circumstellar matter
stars: coronae
stars: distances
stars: dwarf novae
stars: early-type
stars: emission-line, Be
stars: evolution
stars: flare
stars: formation
stars: fundamental parameters
(stars:) gamma-ray burst: general
(stars:) **gamma-ray burst: individual: . . .**
stars: general
(stars:) Hertzsprung–Russell and colour–magnitude diagrams
stars: horizontal branch
stars: imaging
stars: individual: . . .

stars: interiors
stars: jets
stars: kinematics and dynamics
stars: late-type
stars: low-mass
stars: luminosity function, mass function
stars: magnetars
stars: magnetic field
stars: massive
stars: mass-loss
stars: neutron
(stars:) novae, cataclysmic variables
stars: oscillations *(including pulsations)*
stars: peculiar *(except chemically peculiar)*
(stars:) planetary systems
stars: Population II
stars: Population III
stars: pre-main-sequence
stars: protostars
(stars:) pulsars: general
(stars:) **pulsars: individual: . . .**
stars: rotation
stars: solar-type
(stars:) starspots
stars: statistics
(stars:) subdwarfs
(stars:) supergiants
(stars:) supernovae: general
(stars:) **supernovae: individual: . . .**
stars: variables: Cepheids
stars: variables: δ Scuti
stars: variables: general
stars: variables: RR Lyrae
stars: variables: S Doradus
stars: variables: T Tauri, Herbig Ae/Be
(stars:) white dwarfs
stars: winds, outflows
stars: Wolf–Rayet

Interstellar medium (ISM), nebulae

ISM: abundances
ISM: atoms
ISM: bubbles
ISM: clouds
(ISM:) cosmic rays
(ISM:) dust, extinction
ISM: evolution
ISM: general
(ISM:) H II regions
(ISM:) Herbig–Haro objects
ISM: individual objects: . . .
(except planetary nebulae)
ISM: jets and outflows
ISM: kinematics and dynamics
ISM: lines and bands
ISM: magnetic fields
ISM: molecules
(ISM:) planetary nebulae: general
(ISM:) **planetary nebulae: individual: . . .**
(ISM:) photodissociation region (PDR)
ISM: structure
ISM: supernova remnants

The Galaxy

Galaxy: abundances
Galaxy: bulge
Galaxy: centre
Galaxy: disc
Galaxy: evolution
Galaxy: formation
Galaxy: fundamental parameters
Galaxy: general
(Galaxy:) globular clusters: general
(Galaxy:) **globular clusters: individual: . . .**
Galaxy: halo
Galaxy: kinematics and dynamics
(Galaxy:) local interstellar matter
Galaxy: nucleus
(Galaxy:) open clusters and associations: general
(Galaxy:) **open clusters and associations: individual: . . .**
(Galaxy:) solar neighbourhood
Galaxy: stellar content
Galaxy: structure

Galaxies

galaxies: abundances
galaxies: active
(galaxies:) BL Lacertae objects: general
(galaxies:) **BL Lacertae objects: individual: . . .**
galaxies: bulges
galaxies: clusters: general
galaxies: clusters: individual: . . .
galaxies: clusters: intracluster medium
galaxies: distances and redshifts
galaxies: dwarf
galaxies: elliptical and lenticular, cD
galaxies: evolution
galaxies: formation
galaxies: fundamental parameters
galaxies: general
galaxies: groups: general
galaxies: groups: individual: . . .
galaxies: haloes
galaxies: high-redshift
galaxies: individual: . . .
galaxies: interactions
(galaxies:) intergalactic medium
galaxies: irregular
galaxies: ISM
galaxies: jets
galaxies: kinematics and dynamics
(galaxies:) Local Group
galaxies: luminosity function, mass function
(galaxies:) Magellanic Clouds
galaxies: magnetic fields
galaxies: nuclei
galaxies: peculiar
galaxies: photometry
(galaxies:) quasars: absorption lines
(galaxies:) quasars: emission lines
(galaxies:) quasars: general
(galaxies:) **quasars: individual: . . .**
(galaxies:) quasars: supermassive black holes
galaxies: Seyfert

galaxies: spiral
galaxies: starburst
galaxies: star clusters: general
galaxies: star clusters: individual: . . .
galaxies: star formation
galaxies: statistics
galaxies: stellar content
galaxies: structure

Cosmology

(cosmology:) cosmic background radiation
(cosmology:) cosmological parameters
cosmology: miscellaneous
cosmology: observations
cosmology: theory
(cosmology:) dark ages, reionization, first stars
(cosmology:) dark energy
(cosmology:) dark matter
(cosmology:) diffuse radiation
(cosmology:) distance scale
(cosmology:) early Universe
(cosmology:) inflation
(cosmology:) large-scale structure of Universe
(cosmology:) primordial nucleosynthesis

Resolved and unresolved sources as a function of wavelength

gamma-rays: diffuse background
gamma-rays: galaxies
gamma-rays: galaxies: clusters
gamma-rays: general
gamma-rays: ISM
gamma-rays: stars
infrared: diffuse background
infrared: galaxies
infrared: general
infrared: ISM
infrared: planetary systems
infrared: stars
radio continuum: galaxies
radio continuum: general
radio continuum: ISM
radio continuum: planetary systems
radio continuum: stars
radio lines: galaxies
radio lines: general
radio lines: ISM
radio lines: planetary systems
radio lines: stars
submillimetre: diffuse background
submillimetre: galaxies
submillimetre: general
submillimetre: ISM
submillimetre: planetary systems
submillimetre: stars
ultraviolet: galaxies
ultraviolet: general
ultraviolet: ISM
ultraviolet: planetary systems
ultraviolet: stars
X-rays: binaries
X-rays: bursts
X-rays: diffuse background
X-rays: galaxies
X-rays: galaxies: clusters
X-rays: general
X-rays: individual: . . .
X-rays: ISM
X-rays: stars